Detection Algorithm of Aluminum Surface Defects Using Machine Vision

Yang Wu, Jie Liu, Yaqin Zhang, Lianshuang Yu, Jingchun Wu
School of Mechano-Electronic Engineering
Wuxi Taihu University
Wuxi, China,214064
wxwtim@163.com

ABSTRACT
With the growth of global economic and the widespread use of aluminum profile, the consumption of the global aluminum profile increases year by year. In this paper, we proposed a novel detection algorithm of aluminum surface defects using machine vision. Firstly, the aluminum images are acquired and analyzed sequentially, then a number of image processing strategies were used to detect various surface defects. The main contribution is a new area partition method, which can automatically assign texture and no-texture regions with texture information. The proposed method is proven able to detect defects on aluminum profile surfaces, such as cracks, pits, rust or scratches, rapidly and precisely. Robustness and effectiveness in the practical aluminum casting process are improved by using the proposed system.

CCS Concepts
• **Theory of computation → Theory and algorithms for application domains → Machine learning theory → Unsupervised learning and clustering**

Keywords
Aluminum; Machine Vision; Region Segmentation; Surface Defect; Detection

1. INTRODUCTION
In modern production processes, machine vision technology is gradually replacing traditional manual detection methods because of its highly efficient and accurate recognition rate. One of the most important goals of industrial machine vision is to develop computer and electronic systems for quality control (QC) in industrial production processes [1-4]. With the rapid development of digital signal processing and computer techniques, surface defect detection based on machine vision has been used in numerous fields such as the fabric industry [5,6],wood inspection [7], rail defect detection [8], steel defect detection [9] and other applications [10-12]. In this paper, we propose the real-time detection of surface defects in the aluminum casting process using machine vision.

IVSP 2019, February 25–28, 2019, Shanghai, China

ACM ISBN 978-1-4503-6175-0/19/02…$15.00
DOI: https://doi.org/10.1145/3317640.3317661

In industrial aluminum casting, a variety of defects on the surfaces of aluminum profiles may result from the production environment and production process. Therefore, surface defect detection must be conducted before products leave the factory to ensure that defective products are not delivered to the customer. This is done by manual detection currently because artificial on-line recognition has shortcomings. Slow speed, missed readings and non-uniform testing standards can lead to low detection efficiencies, relatively higher labor costs and defective rates, and other production bottlenecks. These problems could be resolved by research into and development of automatic detection technologies for aluminum profiles. Few papers discuss the application of this technology in aluminum production, but a series of defect detection methods has been discussed for other materials and can be used as reference. Yamaguchi [13] presented a crack detection approach based on the percolation model and edge information for large concrete surface images. Fujita [14] proposed a crack detection method for noisy concrete surfaces using probabilistic relaxation and a locally-adaptive threshold. Mandriota [8] applied the k-nearest neighbors algorithm to classify filter responses and wavelet coefficients and detect the presence of surface defects (a particular class) based on the texture analysis of rail surfaces. Santanu [15] developed an automated visual inspection system (which localizes defects by employing kernel classifiers) for an integrated steel plant to capture surface images in real time. Wu [16] proposed a lower envelope Weber contrast recognition method to detect pit defects on steel bar surfaces. Firstly, a lower envelope of column pixels was used to eliminate the effect of high gray level peak value points, and then Weber contrast was used to ensure all areas in one image have the same threshold to detect pit defects. A machine vision system was built in our laboratory to test and evaluate this technique for the defect detection of aluminum profiles.

A novel method based on machine vision to solve the problem of detecting defects on the surface of aluminum profiles is proposed in this work, and image area processing is applied to segment defects. The remainder of the paper is organized as follows. The aluminum casting process and its specific challenges are discussed in Section 2. The surface defect detection method is presented in detail in Section 3. Experimental results for evaluating the method performance are shown in Section 4 and conclusions are presented in Section 5.

2. INDUSTRIAL REQUIREMENTS
As shown in Figure 1, aluminum profile production comprises principal processes including melting, extrusion, anodizing, QC, and packaging. In the melting process, impurities that are sometimes blended in with the aluminum cause final materials not to conform with requirements. Furthermore, bubbles and scratches are often produced in the extruding process, and uneven anodizing

may occur in the anodizing process. Aluminum profiles may therefore have defects such as bubbling, scratches, watermarks, bumps, and stains. Therefore, a QC stage is of great importance in the aluminum casting process to detect defects on the aluminum profile surfaces.

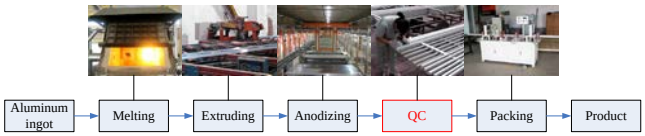

Figure 1. Aluminum profile production processes.

The most difficult task in automatic defect detection over manual inspection is how to distinguish the difference in aluminum profile type during the QC process. Various aluminum product types exist for different applications and each type has its own unique structure and texture. Human beings can easily ignore the structure and texture of the aluminum profiles and only focus on its surface defects. Computers, however, find it difficult to identify whether a pattern is a defect or the texture of the profile. Figure 2 provides examples of different aluminum profile products.

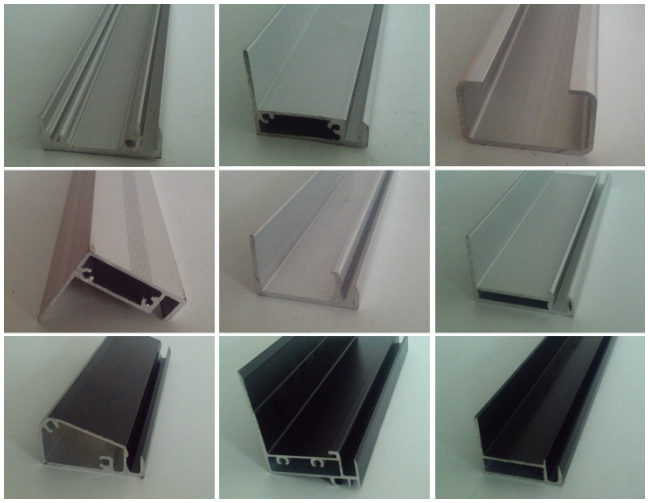

Figure 2. Examples of aluminum profiles.

3. DEFECT DETECTION METHOD

Figure 2 shows that each aluminum profile has unique structure and texture. In our research, we focus on the products which were used as the frame of photovoltaic system and furniture frame. For the use reason, the aluminum surface has some grooves which looks is composed of dense lines area in the plane photos. The surface patterns of the aluminum profile are also composed of some lines. In order to facilitate the description, we unity the region with grooves and patterns collectively referred to as the "texture regions". On the contrary, smooth regions are called "non-texture regions". The boundaries between texture regions and non-texture regions are obvious, horizontal lines can be well separated them. The use of the same algorithm to detect defects on both the texture and non-texture regions would be problematic as texture itself is likely to be mistaken for a defect while some small defects may be hidden in the texture regions that are difficult to detect. The use of different algorithms for the different regions is therefore a better choice.

A two-dimensional (2D) image containing two defects is shown in Figure 3(a). Lines 1 to 5 represent different cross sections. Figure 3(b), (c) and (f) are gray-level profiles across the respective faultless lines 1, 2 and 5 in Figure 3(a) and they have similar structures. Figure 3(d) and (e) are gray-level profiles that cross over the defects in lines 3 and 4, respectively, in Figure 3(a). It is evident that they have different structures and that the gray values of the no-texture area change gradually when there is no defect. Therefore, the first step for the detection of defects in this work is to differentiate textured and non-textured regions in the aluminum using different texture lines.

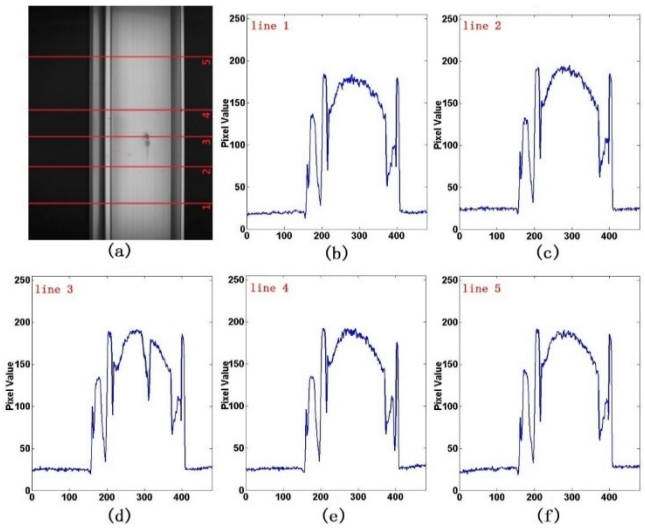

Figure 3. Gray-level of aluminum profiles in different sections.

The detection process is shown in Figure 4. Image preprocessing is conducted first and includes smoothing and enhancement. Image smoothing is used to remove the effects of non-uniform illumination. The purpose of image enhancement is to expand the differences between objects in the image features, emphasize interesting features and suppress irrelevant features. Region segmentation is then conducted and different algorithms are used in different regions (textured and non-textured regions). Finally, defect detection is used to locate defects and connect areas.

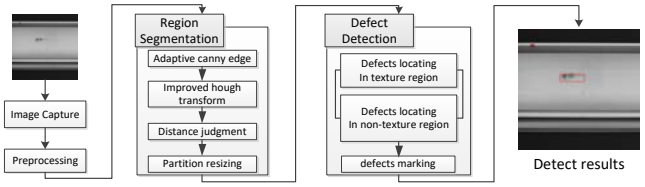

Figure 4. Flow chart of machine vision method for defect detection.

3.1 Adaptive Canny Edge and Improved Hough Transform

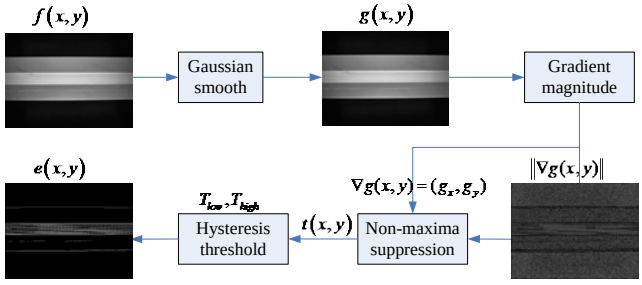

Figure 5. Stages of the Canny algorithm.

Before the region segmentation, edge detection should be done in order to obtain the region boundary. In this paper we use the adaptive threshold Canny edge detection algorithm, including the following steps: Gaussian smooth, gradient magnitude, non-maxima suppression and hysteresis threshold, as shown in Figure 5.

A number of adjustable parameters, such as T_{low} and T_{high} , need to be set up manually in the Canny algorithm. The computational time and effect of the Canny algorithm depend largely on these parameters. Therefore, a novel Canny detector is presented, which employs adaptive selection of double thresholds [17].

Otsu proposed an excellent method for separating foreground from background in images [18]. In his method, the optimal threshold is automatically selected by maximizing the inter-class variance based on a gray-level magnitude histogram. Threshold segmentation is used to select the best threshold by obtaining two thresholds with best separability between classes. This is considered to be optimal mathematical statistics in the sense of maximum variance between classes and minimum variance within the class [18]. In this paper, Otsu's method based on the gradient magnitude histogram is used to calculate the upper threshold for the new Canny detector and the ratio of the lower to upper threshold is 0.4.

The standard Hough transform is an effective method for implementing line detection in a binary image. In this method, points in the xy-plane are mapped to points in the parameter space. The Hough transform was proposed by Paul Hough [19] in 1962 and Richard Duda and Peter Hart popularized its use in 1972 [20]. The Standard Hough transform is tolerant of gaps in feature boundary descriptions and is relatively unaffected by image noise, but intensive computation and large memory storage capabilities are required. There is a number of existing methods to improve the performance of the Hough transform [21,22]. In our application, testing aluminum texture is level approximately and thus the constraint θ is $\left(\frac{17\pi}{18},\frac{19\pi}{18}\right)$. θ will be discretized into five parameter space, which can greatly reduce the calculation cost and improve the running speed.

3.2 Region Segmentation

Since our objective is to develop online detection system, so the system needs to have certain flexibility. If the partition information of each type were written in advance, then in the testing work, if there was a slight deviation in through the equipment, it will cause the image displacement and matching error. To avoid this situation, our strategy is to do region segmentation every time a batch of tested material type was changed. The process of region segmentation algorithm is as follows:

Before defecting, we used the first th frame pictures to conduct region segmentation. The threshold th indicates how many frames we want to use.

Use adaptive threshold Canny operator to detect the edge of first image and then obtain binary image.

Use improved Hough transform for each pixel in the binary image and save the line that satisfies the following conditions:

$$line_i = sline_n \qquad \text{if } WP_n > Pth \tag{1}$$

Where $sline_n$ is the nth line detected by Hough transform, WP_n is the number of white points, Pth is a threshold, which is half of the image width. That is to say, the line will be discarded if it is shorter than half of the image width.

Sort the lines according to increase in vertical ordinate at the center. The lines are denoted $line_0, line_1, \cdots line_{m-1}$, after sorting satisfying $cv_0 < cv_1 < \cdots < cv_{\text{m-1}}$. cv_t is the vertical ordinate of the line $line_t$ center and m is the number of lines.

Divide regions according to the straight line of the first frame image: assign the first vertical ordinate to be the starting and closing position of the first texture region. Starting from the second line, if the distance between the vertical ordinate of the current and front line centers are less than the threshold value, then expand the texture region. Alternatively, conclude that the current line is not in the same texture region with the front line and then make the vertical ordinate of the current line center the starting and closing position of the next texture region. As shown in (2):

$$\begin{cases} R_{ie} = cv_j & if \left| cv_j - cv_{j-1} \right| < Dth \\ R_{(i+1)s} = R_{(i+1)e} = cv_j & else \end{cases} \tag{2}$$

where $R_{is}$and $R_{ie}$are the starting and closing coordinates of the ith texture region, cv_j is the vertical ordinate of the line $line_j$ center, Dth is threshold of the distance between two adjacent lines with a value of 10 in the experiment.

Starting from the second frame, compare the detected line with all divided regions. If the distance between the vertical coordinate of the line center and some divided region is less than the threshold value, then merge the line into this region:

$$\begin{gathered} if\ \left(cv_j > R_{is} - Lth\ \&\&\ cv_j < R_{ie} + Lth\right) \\ \begin{cases} R_{is} = min(cv_j, R_{is}) \\ R_{ie} = max(cv_j, R_{ie}) \end{cases} \end{gathered} \tag{3}$$

Where Lth is the distance threshold between line and area, and is equal to 10 here.

If the distances between the vertical coordinate of the line center and all divided texture regions are no less than the threshold value, then the straight line is considered to be a new texture region:

$$R_{as} = R_{ae} = cv_j \tag{4}$$

If the frame is the last image, according to the divided texture areas, combine the overlapping area and remove the area that has fewer occurrences than half of the frames used in the area partition, then expand the texture areas and determine the textured and non-textured regions of the aluminum profile.

A schematic region segmentation diagram is shown in Figure 6. Figure 6(a) is the original image of the aluminum surface. Figure 6(b) is the binary image using Canny operator edge detection. The white pixels are the detected lines, while the background is black. In Figure 6(c), the red straight lines are consistent with the condition resulting from the Hough transform and the green dot is denoted as the line center. Figure 6(d) is the result of segmentation and the whole testing range is divided into three regions, which are termed area1(green texture area),area2(blue no-texture area)and area3(green texture area).

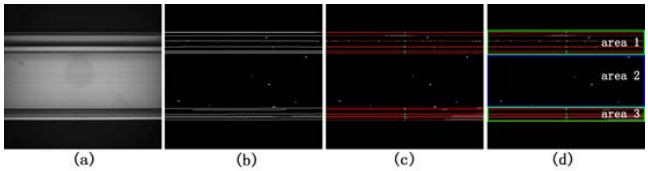

Figure 6. Area partition schematic diagram.

3.3 Defect Detection

In this paper, defects can be defined as a group of pixels distinct from a group of background pixels. The difficulty in obtaining an optimal boundary between two groups is termed a binary classification problem. The defect area can be divided by selecting a proper threshold value. An example of the defect detection process is shown in Figure 7. When the defect area is determined, the size of the defect is measured. An original defect image is shown in Figure 7(a).Three-dimensional (3D) and 2D profiles are illustrated in Figure 7(b) and(c), respectively. The central cross-sectional area in Figure 7(d) is considered to be a different area. The dimension of the upper cross-sectional area is measured and the results are dependent on the choice of threshold value. A conventional choice of threshold value is termed the valley-emphasis method. The objective of automatically selecting the threshold value is to obtain the valley in the histogram that separates the foreground from the background, as illustrated in Figure 8. The gray values for the green and red lines are 130 and 170, respectively.

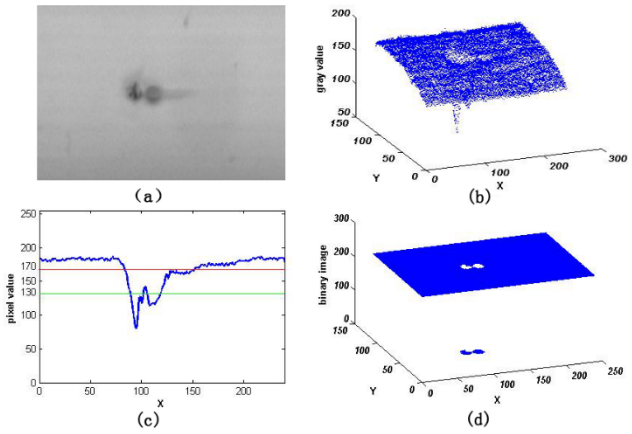

Figure 7. Comparison of defect image

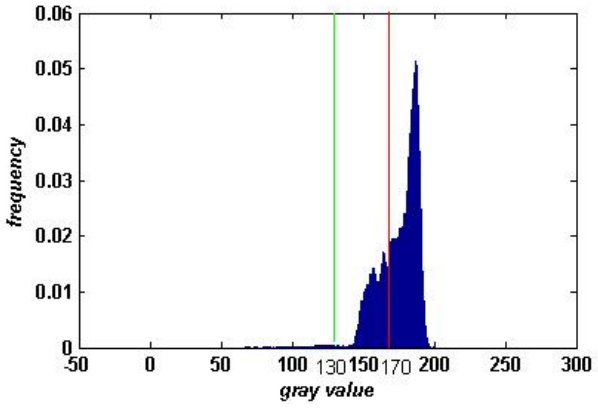

Figure 8. Histogram of defect image.

3.4 Defect Marking

When the defects are located successfully, we need to highlight the defective area with a brightly colored marked box that is easily visible to the inspectors. The process is shown in Figure 9. Figure 9(a) is a binary figure which needs to be marked. The values of each corresponding pixel coordinate are shown in Figure 9(e), where a value of 1 indicates prospective points and 0 denotes a background point. Eight interconnected regions are used, and the image is scanned from top to bottom and left to right. The following situations are considered for each pixel in the image:

(1) As shown in Figure 9(b), point A is an unmarked foreground point. The left and topside of point A are background or prohibited access points. This indicates that point A is on the outer boundary of some connected domain. A new label is given to pixel point A (the labels of the connected domain start from 2). The eight neighborhood search method is used to track, in a clockwise direction, the area outside the outline across pixel point A and to mark the same label as pixel point A. All background points that are neighborhoods of the outside outline are marked -1, and denote prohibited access points, as shown in Figure 9(f).

(2) As shown in Figure 9(c), point B is an unmarked foreground point. The left side of point B is a foreground point and has been marked. The label to the left of the foreground point has been copied to the current point B, as shown in Figure 9(g).

(3) As shown in Figure 9(d), the right side of the marked foreground point C is a background, which shows that pixel point C is on the internal boundary of some connected domain. The eight neighborhood search method is used to track, in an anticlockwise direction, the area internal to the outline across pixel point C and to mark the same label as pixel point C. All background points that are neighbors to the internal outline are marked -1, which denotes prohibited access points.

In Figure 9(d), point D is processed according to above step 2 and is labeled as 2. This is the same as the left marked foreground point shown in Figure 9(h). Therefore, the labels of the entire marked connected domain are assigned a value of 2.

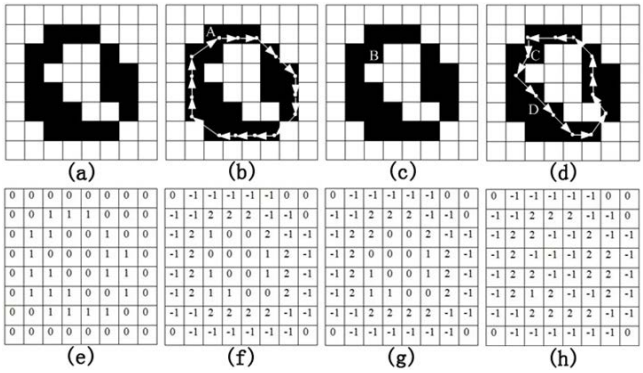

Figure 9. Connected area labels diagram.

As shown in Figure 10, serial number1-3 is a binary image with 352 × 288 pixels and 800 sample points of type number 1 are included in the connected area. Serial number 2 contains 120 irregular “U”-type shapes in the connected area and nine circular connected areas with 25 × 25 pixels are included in number 3. Serial number 4 contains 9 squares which size is 25 × 25 pixels. Serial number 5 contains 9 ovals with 30 pixels major axis and 20 pixels minor axis. Serial number 6 is a binary image with 640 × 480 pixels and contains four irregular connected are as with larger area. Figure 11 shows a comparison of the running time for

several labeling methods. The traditional sequential labeling method has a low efficiency because two scans are required and it is necessary to solve the label conflict. It therefore struggles to meet the real-time application requirements. The linear labeling method is sensitive to the shape of the connected regions. The depth and breadth optimization search methods are not sensitive to the shape of the connected region but are sensitive to the area of the connected region. Therefore, these methods can only be applied to small connected areas. The proposed method in this paper is insensitive to the shape and size of the connected area and has very good robustness.

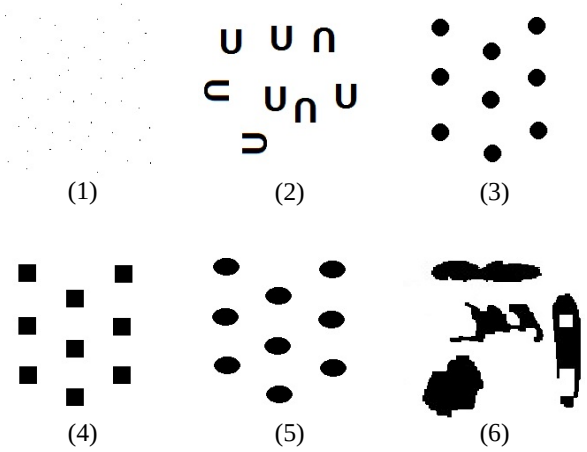

Figure 10. Different sequence for test running time.

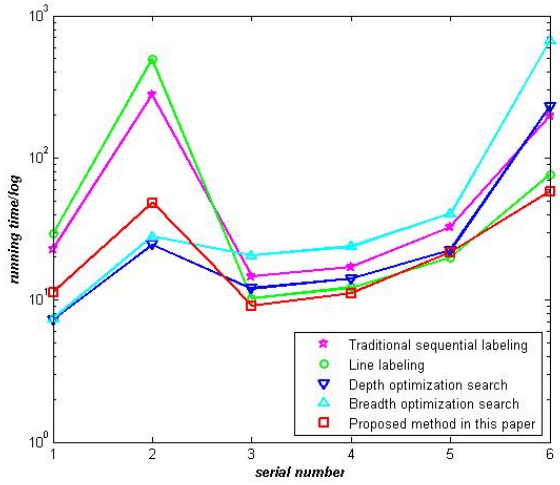

Figure 11. Running time for several labeling methods.

4. EXPERIMENT

4.1 Process Description

A hardware platform for testing the proposed detection method has been built. The design of the platform can facilitate the capturing of high-quality images of the aluminum profiles. An aluminum transfer roller is used to transport the aluminum profiles. Image acquisition and processing is achieved using the intelligent camera unit. Figure 12(a) shows a photograph of the laboratory prototype and Figure 12(b) is the design drawing with supporting frame(1), lighting module(2), image acquisition module(3),alignment sensor(4), conveying module(5), and computer(6).

The roller systems located on both sides of the prototype inspection system are designed to ensure smooth and even movement of the aluminum sample. Motor rotation is controlled by a motion control board which can adjust the conveying speed. Three degrees-of-freedom movement is provided to the camera by the designed system and allows the photo sensor array of the intelligent camera and dome light source to align in the same plane. An extra degree-of-freedom is provided for changing the vertical distance between the camera and the aluminum sample to adjust the resolution along the selected direction. Intelligent cameras produced by the Germany Vision Components Company were used in the image acquisition module. Their resolution is 640 × 480 with a frame rate of 32 FPS. The VC4018 is shock resistant, has a strong impact resistance capability, and integration of the RS-232, 100MB Ethernet, and multi-channel digital I/O hardware interface can meet the demands of various industrial machine vision systems. The dome lighting source provides sufficient uniform light to eliminate brightness and shadows and is an ideal choice for shiny and curved surfaces. The supply of multi-angle light on the field of view is provided by a divergent hemispherical design.

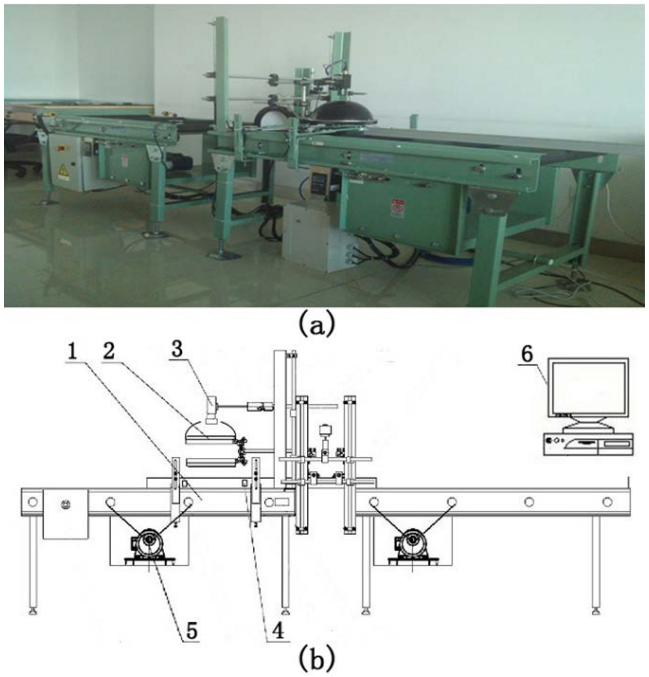

Figure 12. Architecture of vision inspection system.

4.2 Experimental Results

Certain detection results for the aluminum profile images in the database are presented in Figure 13. Sample images of aluminum profiles with different defect types are shown in Figure 13(a), including bubbling, scratches, watermarks, stains, etc. The region segmentation results are shown in Figure 13(b), where the green rectangles show texture areas and the blue rectangles are no-texture areas. The defect binary images are shown in Figure 13(c). In Figure 13(d), results have been processed using morphological operations. Final defect results obtained using the proposed method are shown in Figure 13(e). Defects can be readily detected using the proposed method and the defects can also be segmented accurately using the proposed scheme.

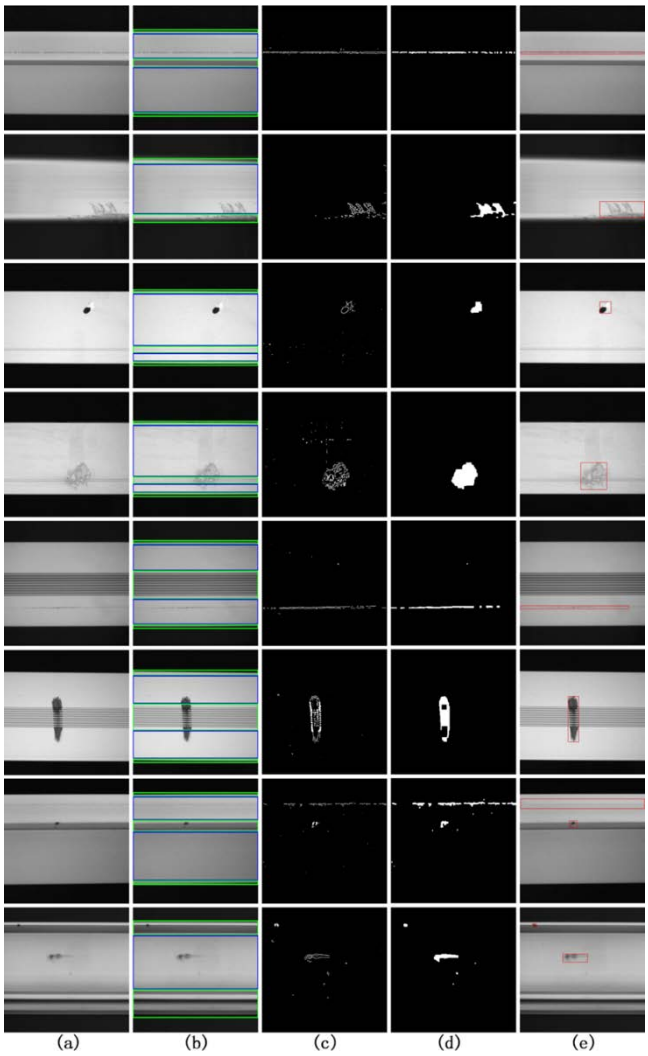

Figure 13. Defect detection results.

4.3 Method Contrast

A total of 160aluminum profiles, containing 156 silver aluminum profiles and 4 black aluminum profiles, were used for detecting defects. Of these, 30were without defects and 130 profiles contained 193 defects.

Sensitivity and specificity are statistical measures of the performance of a binary classification test, also known in statistics as classification function. They are defined as:

$$\text{sensitivity} = \frac{TP}{TP + FN}$$

$$\text{specificity} = \frac{TN}{TN + FP}$$

where TP is true positives, FN is false negatives, TN is true negatives, FP is false positives.

A comparison of various edge detection methods in Table 1 shows that the proposed method is superior. Table 2 shows the parameter of comparison detection methods.

Table 1. Comparison of several edge detection methods

	Sensitivity	Specificity	Detection time(ms)
Proposed method	0.927	0.958	165
Gabor Wavelet	0.938	0.953	258
Roberts edge	0.835	0.852	102
Sobel edge	0.881	0.898	132
Laplace edge	0.896	0.911	124
Laplace of Gaussian edge	0.907	0.928	144
Canny edge	0.917	0.945	157

In defect detection work for aluminium, the so-called defects in the picture are the pixels which have intense contract with the surrounding pixels in fact, especially for the edge of the defect area. So, edge detection methods are usually the most directly and effectively method to detect defects. The comparison methods in Table 1 are some state of the art methods which used in other defect detection work [1][2]. There are some other methods which are used to detect surface defects such as [3], [4] and [5]. But these method are not suitable for our application because of the real-time demand (running four cameras at the same time).

Table 2. Parameter of comparison detection methods

	Size	Detail
Roberts	2*2	{1,0;0,-1};{0,1;-1;0}
Sobel	3*3	{-1,-2,-1;0,0,0;1,2,1}; {-1,0,1;-2,0,2;-1,0,1}
Laplace	3*3	{0,-1,0;-1;-1,4,-1;0,-1,0}
LoG	5*5	{-2,-4,-4,-4,-2;-4,0,8,0,-4; -4,8,24,8,-4;-4,0,8,0,-4;-2,-4,-4,-4,-2}

In the experiments, Gabor transform achieved good results. The result has accurate location, clear edge and effective noise smoothing. However, as four different direction filters were used to do convolution operation, it has long calculating time which can't meet the needs of real-time detection. Roberts edge algorism is simple and fast in speed of operation. But this method is sensitive to noise, insensitive to fuzzy edge, so the detection result is not acceptable. There are some fake edges when using Soble edge algorism and the location of edge was not accurate. Laplace operator is a second derivative operator for two-dimensional function, are always used with Gaussian filter. The results of this method are somewhat incomplete when edges and background are not in strong contrast. Canny method can detect not only the edges we want but also many superfluous results. The method proposed in this paper achieves a high sensitivity, high specificity and high recognition speed.

5. CONCLUSION

In this paper, a novel surface defect detection method based on machine vision is presented for aluminum profiles. Machine vision is a potential alternative for replacing unreliable manual detection. Visual defects are fully explored and a detection method that can automatically learn aluminum edges has been developed. Experimental results indicate that the defect detection method is promising for obtaining defect data with application in the real-time manufacturing environment and in-line tests are currently underway. The proposed system can be used to improve the consistency of product quality and reduce production costs in the aluminum casting industry. With further analysis and experiments, the proposed method can be applied to research into detecting other defects.

6. REFERENCES

[1] Levitt T S, Agosta J M, Binford T O. Model-Based Influence Diagrams for Machine Vision[C]// *Conference on Uncertainty in Artificial Intelligence*. North-Holland Publishing Co. 1990:371-388.

[2] Binford T O, Levitt T S, Mann W B. Bayesian Inference in Model-Based Machine Vision[C]// UAI '87: *Proceedings of the Third Conference on Uncertainty in Artificial Intelligence*, Seattle, Wa, Usa, July. DBLP, 2013:73-96.

[3] Davies E R. Computer and machine vision: theory, algorithms, practicalities[M]. *Academic Press*, 2012.

[4] Carrasco M, Mery D. Automatic multiple view inspection using geometrical tracking and feature analysis in aluminum wheels[J]. *Machine Vision & Applications*, 2011, 22(1):157-170.

[5] Chetverikov D, Hanbury A. Finding defects in texture using regularity and local orientation[J]. *Pattern Recognition*, 2002, 35(10):2165-2180.

[6] Shi M, Jiang S, Wang H, et al. A Simplified pulse-coupled neural network for adaptive segmentation of fabric defects[J]. *Machine Vision & Applications*, 2009, 20(2):131-138.

[7] Silvén O, Niskanen M, Kauppinen H. Wood inspection with non-supervised clustering.[J]. *Machine Vision & Applications*, 2003, 13(5-6):275-285.

[8] Mandriota C, Nitti M, Ancona N, et al. Filter-based feature selection for rail defect detection[J]. *Machine Vision & Applications*, 2004, 15(4):179-185.

[9] Huang X Q, Luo X B, Wang R Z. A real-time parallel combination segmentation method for aluminum surface defect images[C]// *International Conference on Machine Learning and Cybernetics. IEEE*, 2015:544-549.

[10] Blasco J, Aleixos N, Moltó E. Computer vision detection of peel defects in citrus by means of a region oriented segmentation algorithm[J]. *Journal of Food Engineering*, 2007, 81(3):535-543.

[11] Jacob Borg, Samuel Gershon, Murray Alpert. Optimal Gabor filters for textile flaw detection[J]. *Pattern Recognition*, 2002, 35(12):2973-2991.

[12] Tsai D M, Wu S C, Li W C. Defect detection of solar cells in electroluminescence images using Fourier image reconstruction[J]. *Solar Energy Materials & Solar Cells*, 2012, 99(99):250-262.

[13] Yamaguchi T, Hashimoto S. Fast crack detection method for large-size concrete surface images using percolation-based image processing[J]. *Machine Vision & Applications*, 2010, 21(5):797-809.

[14] Fujita Y, Hamamoto Y. A robust automatic crack detection method from noisy concrete surfaces[M]. *Springer-Verlag New York*, Inc. 2011.

[15] Ghorai S, Mukherjee A, Gangadaran M, et al. Automatic Defect Detection on Hot-Rolled Flat Steel Products[J]. *IEEE Transactions on Instrumentation & Measurement*, 2013, 62(3):612-621.

[16] Li W B, Lu C H, Zhang J C. A lower envelope Weber contrast detection algorithm for steel bar surface pit defects[J]. *Optics & Laser Technology*, 2013, 45(1):654-659.

[17] Lv M, Su H, Li Y. An Adaptive Canny Detector with New Differential Operator[C]// *International Conference on Wireless Communications NETWORKING and Mobile Computing. IEEE*, 2010:1-4.

[18] N. Otsu. A threshold selection method from gray-Level histogram[J]. *IEEE Transactions on Systems Man and Cybernetics*, 1979, 9(1):62-66.

[19] HOUGH,P. V. C. Method and means for recognizing complex patterns[J]. 1962.

[20] Duda R O. Use of the Hough transformation to detect lines and curves in pictures[J]. *Communications of the ACM*, 1972, 15(1):11-15.

[21] Ghazali K, Xiao R, Ma J. Road Lane Detection Using H-Maxima and Improved Hough Transform[C]// *Fourth International Conference on Computational Intelligence, Modelling and Simulation. IEEE*, 2012:205-208.

[22] Bendale A, Nigam A, Prakash S, et al. Iris Segmentation Using Improved Hough Transform[J]. 2012.